POSTFIRE PERFORMANCE OF GFRP STAY-IN-PLACE FORMWORK FOR CONCRETE BRIDGE DECKS

Journal Paper

ASCE Journal of Composites for Construction, *Vol. 23 Issue 3*

Nicoletta, B., Woods, J., Gales, J., Fam, A.

June 2019

DOI: 10.1061/(ASCE)CC.1943-5614.0000941

John Gales (Principal Investigator, York University)
Benjamin Nicoletta (Graduate Student, York University)
Joshua Woods (Graduate student, Carleton University)
Amir Fam (Professor, Queen's University)

Abstract

This study focuses on the fire performance of glass fiber–reinforced polymer (GFRP) stay-in-place structural formwork used for the rapid construction of reinforced concrete (RC) bridge decks and serves to direct future studies on the matter. Seven beam sections of a concrete deck reinforced using a GFRP stay-in-place form are tested. The beams in this study are subjected to both fire and simulated-fire damage and tested in four-point bending to assess the mechanical contribution of the GFRP stay-in-place formwork. Fire damage was applied to one beam via a 14.5-min heptane pool fire. Experimental results show that the simulated damage was an overly conservative representation of the fire damage sustained. The fire damage was insufficient to reduce the ultimate load or change the failure mode of the specimen when compared to an undamaged control. The embedded T-rib of the GFRP form was protected from fire damage and provided redundancy to the system. Despite a char thickness of about 15% of the base thickness, the GFRP base plate was able to protect the adjacent concrete from temperatures exceeding 100°C. An increased flexural capacity was observed in the fire-damaged specimen hypothesized to be a result of concrete precompression arising from the heating and cooling of the GFRP formwork. A series of direct bond shear tests between GFRP–concrete samples at elevated temperatures found a decrease in bond shear stress and bond stiffness as bond temperatures increased.

Table of Contents

1. Introduction

Bridges represent some of the most critical infrastructure in society, acting as vital transportation links for the movement of people and goods. The rapid development of transportation infrastructure, combined with an increasing volume of transported hazardous/ flammable materials, makes bridge fires a widespread concern (Garlock et al. 2012). Although rapid evacuations of bridge spans during fires allow life safety objectives to be met relatively easily, the materials and structural systems of bridges are rarely designed to limit economic losses, which can be substantial in the event of bridge closure or collapse.

In recent years, there has been a rise in the use of advanced composite materials such as glass fiber–reinforced polymers (GFRPs) in civil engineering applications. One innovative application of GFRP composites is the use of stay-in-place permanent formwork for reinforced concrete (RC) structural elements. The benefits of pultruded GFRP composite formwork include a high strength-to-weight ratio, resistance to corrosion, availability in a variety of configurations, and reduced construction time when compared to traditional formwork. Specifically, the corrosion resistance and reduced labor have made pultruded GFRP stay-in-place formwork popular in bridge deck construction where harsh environments will accelerate the corrosion of steel reinforcement (Nelson and Fam 2014a).

In past research, many GFRP stay-in-place cross sections have been studied for bridge deck applications, including protruding box sections, hollow cavities, and corrugated sheets (Nelson and Fam 2013, 2014a, b). This paper focuses on a GFRP stay-in-place form that features a base plate with T-shaped ribs protruding upward, aptly named T-Up formwork. The T-Up ribs in this variation span the deck transversely to traffic and between girders. Due to the limited width of forming dies in the pultrusion process, GFRP stay-in-place forms are designed to be spliced together with mechanical or adhesive fasteners. Fig. 1 demonstrates a typical span of a bridge deck reinforced with the spliced GFRP formwork used in this study. GFRP stay-in-place forms are built in the same manner as traditional formwork but remain composite with the concrete as part of the structural member. In this configuration, the underside of the bridge deck and GFRP soffit is exposed to damage from fire or vandalism from below.

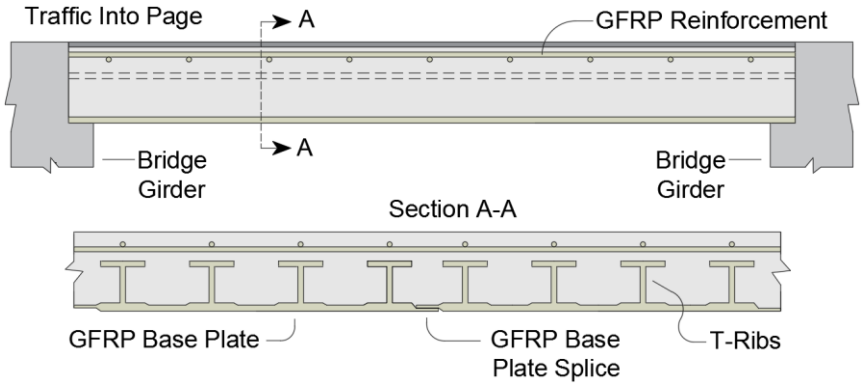

Fig. 1. Typical configuration of GFRP stay-in-place T-up formwork.

Due to the variable nature of GFRP fabrication, there exists an extremely wide variety of structural applications, many of which have not yet been studied in terms of fire performance. Despite the numerous structural applications of GFRPs, previous studies investigated the mechanical behavior, fire resistance, and modeling strategies of pultruded GFRP members including bridge decks, beams, and columns, among others (Correia et al. 2010, 2013, 2015; Gibson et al. 2006; Bai et al. 2010; Morgado et al. 2015, 2018a, b; Yanes- Armas et al. 2016, 2017). Little to no fire testing has been conducted in connection with GFRP stay-in-place formwork systems. In general, the lack of information affecting some GFRP applications' performance in fire is a major issue inhibiting their widespread use (Morgado et al. 2015). To the authors' knowledge, this study is the first fire exposure test involving a concrete-GFRP stay-in-place formwork member, and for this reason, conducting an extreme in-fire test with no prior knowledge of the system's response to fire might be premature. Ultimately this study focuses on the mechanics of a fire-damaged GFRP system in order to provide direction for future studies that will consider a wider variety of in- and postfire testing with more severe damage and aim to establish fire resistance ratings for the system. This research aims to examine the structural contribution of GFRP stay-in-place formwork in a bridge deck that has been damaged by a small pool fire from below. Fire damage is also simulated in varying spans to allow for a direct analysis of the GFRP stay-in-place formwork's structural contribution.

2. Background and Motivation

The structural performance of GFRP stay-in-place formwork in applications for RC bridge decks has been studied in detail in the literature, and researchers have successfully examined failure modes, behavioral mechanics, the effect of form splicing, and the impact of freeze–thaw cycles (Nelson and Fam 2014a, b, 2013; Boles et al. 2015; Honickman et al. 2009). However, little to no large or small-scale testing has been done to quantify the structural impact of fire damage on GFRP stay-in-place forms.

In terms of mechanical performance, the material's glass fibers have been shown to retain strength at relatively high temperatures. The GFRP in this study uses E-glass fibers, which have a softening temperature of approximately 850°C (Correia et al. 2015). However, the GFRP's polymer resin is more sensitive to high temperatures than the glass fibers due to the effect of glass transition, an important parameter influencing the fire performance of GFRP composites. Glass transition temperature is the temperature at which a resin matrix transitions from a solid to a soft rubberlike consistency and loses its mechanical strength. For many GFRP composites this temperature is typically between 60°C and 140°C (Correia et al. 2013). After exceeding this temperature, composite action between the glass fibers and the epoxy resin is guaranteed to be lost if not already compromised before such a point, reducing the stiffness of the GFRP (Correia et al. 2015). If temperatures increase further and reach the decomposition temperature, the GFRP resin may ignite if it is exposed and has vaporized, potentially contributing to the growth of a fire under specific conditions (Gales et al. 2016). While some more chemically advanced composites can yield strong performance in fire, these hazards can be especially prevalent in economical and chemically simple GFRPs.

In addition to the research needs on this topic, this research was preceded by a material study conducted by Gales et al. (2016), which used a cone calorimeter to test several commercially available GFRP stay-in-place formwork samples and determine fire reaction characteristics. These parameters are of particular interest in bridge applications because the GFRP form makes up the soffit of the bridge deck and could be exposed to fire from below. Fig. 2 below demonstrates the typical burning sequence of the GFRPs in the cone calorimeter tests. The underlying glass fiber structure can be seen as the GFRP resin decomposes, vaporizes, and ignites. After flame-out, a char layer was observed in all tests. Table 1 gives the material and fire reaction properties for the GFRPs used in the study (Gales et al. 2016). Sample 1C is the GFRP material discussed herein and was tested by the authors in accordance to the former test program. Samples 1A, 1B, and 1C were all specified to contain no fire retardants; however, a scanning electron microscope (SEM) microstructural analysis with energy dispersive spectroscopy indicated that Samples 1A and 1B may have contained an active fire retardant agent despite manufacturer specifications. This agent is hypothesized as an aluminum trihydroxide filler. A previous study using the same GFRP stay-in-place formwork as this program found the glass transition temperature of the material to be 109°C when tested in accordance with ASTM E1356-08 (Fam et al. 2016). As shown in Table 1 and as observed by Gales et al. (2016), GFRP thickness plays an important role in the heat transfer, vaporization, and fire chemistry of a sample. A thermally thick sample demonstrates a longer time for the resin to decompose and ignite. Gales et al. (2016) hypothesized that, in the case of a thermally thick GFRP plate heated from below (a typical configuration for a GFRP stay-in-place formwork bridge deck), the resin is likely to decompose and fall off of the structure before igniting in place and influencing fire spread.

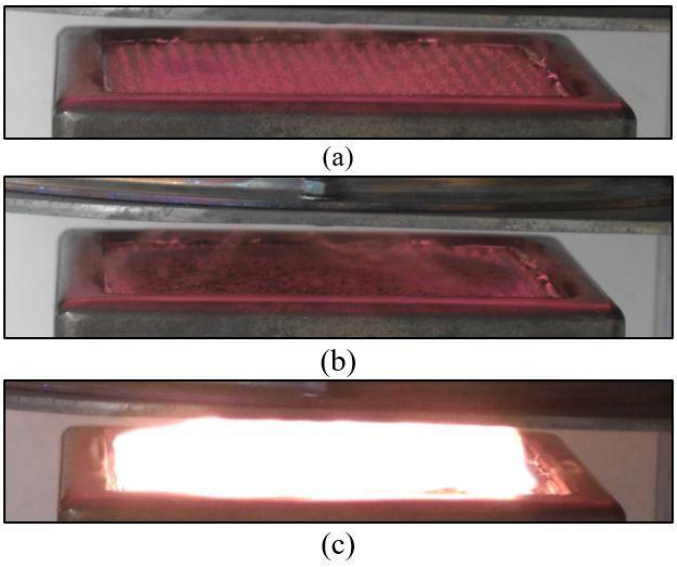

Fig. 2. GFRP stay-in-place formwork cone calorimeter testing sequence: (a) decomposition of GFRP resin; (b) resin vaporization; and (c) ignition.

3. Experimental Program

3.1 Test Specimens and Fabrication

An experimental program was developed to quantify the structural contribution of damaged GFRP stay-in-place T-Up formwork in one-way bending. The test specimens represent strips of concrete bridge deck reinforced with GFRP formwork, created by dividing two full-sized, commercially available GFRP stay-in-place forms longitudinally along the span of the T-ribs. The two 1,675 × 840 mm GFRP forms used in this study each had four T-Up ribs spanning the full length of the forms spaced at 205 mm on center. Gales et al. (2016) determined that the thermal thickness began to influence the samples at approximately 9.5 mm thickness. Thermal thickness has implications for the scalability of fire tests involving GFRPs because the fire resistance properties do not scale proportionally between a thermally thin and thermally thick sample. For this reason, a GFRP thickness greater than 9.5 mm was used in this study to make use of the fire resistance benefits associated with thermal thickness and select a GFRP structural form that was representative of a full-scale bridge deck in practice. The base plate has a maximum thickness of 19 mm, which tapered to 13.7 mm away from the ribs. The ribs protruded 96 mm from the interior of the base plate to the top of the rib flange. Mechanical testing by previous authors measured the ultimate tensile strength and modulus of the GFRP in the longitudinal direction to be 203 MPa and 16.8 GPa, respectively, and the same properties in the transverse direction to be 126 MPa and 15.6 GPa, respectively (Nelson and Fam 2013).

A two-dimensional grid of 10-M GFRP V-ROD rebar was added to each specimen to better represent actual strips of a GFRP stay-in-place formwork bridge deck where a top rebar mesh would be used. The longitudinal rebar was placed 35 mm above each T-Up rib. The transverse bars were the lower rebar layer and spaced at 185 mm. The total beam height including the GFRP base plate was 186 mm. The specimen sizes are based on the dimensions from a full-scale comparison of a RC–steel composite bridge deck with a GFRP stay-in-place formwork–RC bridge deck (Nelson and Fam 2013). The GFRP formwork decks were designed to be comparable to a Canadian Highway Bridge Design Code (CAN/CSA-S6-14)– compliant RC–steel composite bridge deck, resulting in a GFRP member depth of 186 mm to achieve the same effective reinforcement depth as the traditional steel composite deck. However, the GFRP deck had a higher reinforcement ratio and additional vertical ribs compared with the traditional RC–steel deck (Nelson and Fam 2013). The concrete beam widths were chosen as the same spacing of the GFRP T-Up ribs to accommodate and center one full rib per beam (with the exception of C2). The beams and test cylinders were covered by wet burlap for the curing duration. The 50-day concrete compressive strength was 45.7 _ 1.2 MPa based on six cylinders tested in accordance with ASTM C39. The 90-day concrete compressive strength was measured as 47.9 MPa. Fig. 3 shows the strip specimens in the formwork prior to casting and the cured beams. No surface preparation of any kind was applied to the GFRP formwork prior to casting.

The control specimens, referred to as C1 and C2, were tested in their undamaged state and had one and two T-Up ribs along their length, respectively. The purpose behind varying the number of T-Up ribs along the width of the specimens was to determine whether downscaling the

number of T-Up ribs had a proportional effect on the performance of the beam. The beam specimens with simulated fire damage are referred to as SD1, SD2, SD3, and SDF. Simulated damage was applied to these specimens by physically removing the GFRP base plate in different regions of the beam. The T-Up ribs, which were fully embedded in concrete, remained undamaged. Fig. 4 and f outline the dimensions and damage areas of each beam. The basis for the removal of the GFRP base plate originated from the material testing described in Gales et al. (2016), where it was hypothesized that during a fire, a portion of the GFRP base plate would be damaged while the interior T-Up ribs would be protected by the concrete heat sink. This study assumed a worst-case scenario, where the entire thickness of the base plate loses structural capacity. This approach also assumed that the concrete directly adjacent to the base plate remains undamaged from the fire (this is proven valid for the fire scenario in this study). Even if overly conservative, this method of simulating fire damage allows controlled and precise removal of the GFRP base plate, which enabled a better understanding of its contribution to the load carrying capacity of the structural member. The fire-damaged specimen, referred to as FD, was exposed to a 14.5 min heptane pool fire between point loads to compare with Beam SD3, which had simulated damage in the same region. The heated region on Beam FD represented 33% of the beam's span. Two layers of gypsum board were provided outside of the heated zone to prevent flame spread and protect other regions of the beam. The gypsum board was CertainTeed Easi-Lite Lightweight gypsum and had a thickness of 12.7 mm, a weight of 6.4 kg=m2, and both a flame spread rating of 15 and smoke developed rating of 0 in accordance with ASTM E84. After testing and board removal there was no evidence of GFRP damage beneath the boards (no charring/discoloration). This method allowed a direct comparison of the flexural behaviors of Beams FD and SD3.

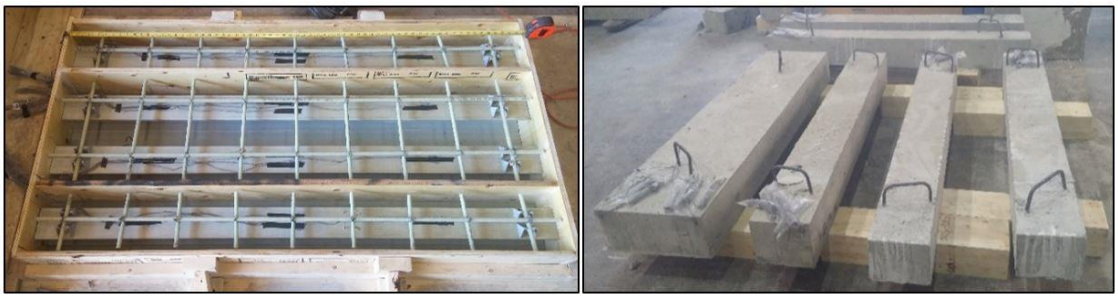

Fig. 3. Beam fabrication and casting.

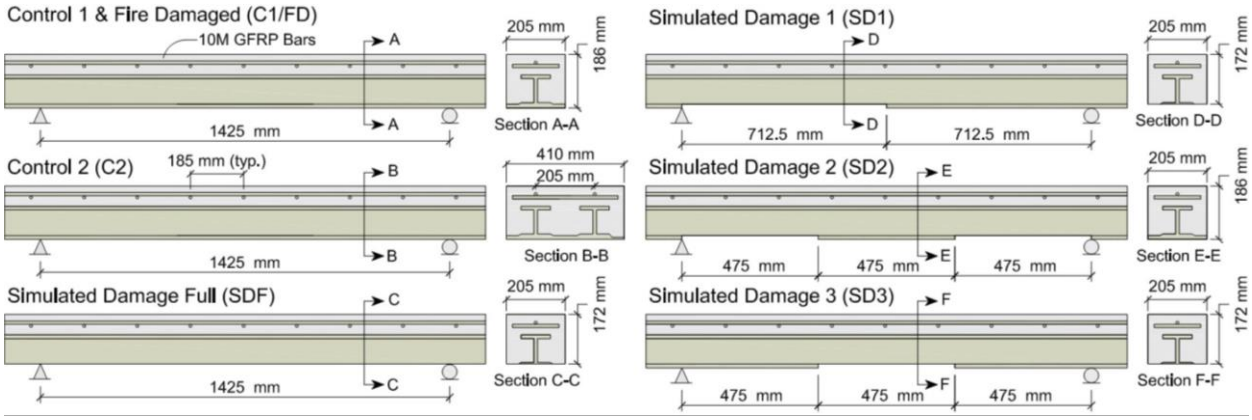

Fig. 4. Control and simulated damage beam specimens.

Table 1. GFRP stay-in-place formwork test configurations and selected fire reaction polymer test results with 50 kW/m^2 incident heat flux. Adapted from Gales et al. (2016).

Sample	Test Configuration			Test Results			
	Resin Type	Manufacturer Specified Fire Retardant	Thickness (mm)	Ignition Time (s)	Flameout Time (s)	Mass at Ignition (g)	Mass after Flameout (g)
1A	Polyester	No**	3.6	72	410	77.8	55.3
				67	423	76.9	55.2
1B		No**	9.5	187	1091	180.0	129.2
1C*		No	13.7	91	1875	235.0	157.2
				109	1880	235.0	161.0
2A		Yes	6.1	80	671	111.0	73.1
				97	619	110.7	72.2
3A	Vinylester	Yes	4.1	86	300	62.5	38.5
				109	411	60.1	36.5

* GFRP stay-in-place formwork used in this study.
** may have contained an active fire retardant despite manufacturer specification.

Table 2. Test specimen design details.

Beam	Dimensions (mm)	Damage Type
C1	1425 x 205 x 186	None
C2	1425 x 410 x 186	None
SD1	1425 x 205 x 186	Left half of GFRP base plate removed
SD2	1425 x 205 x 186	GFRP plate shear spans removed
SD3	1425 x 205 x 186	GFRP plate removed between point loads
SDF	1425 x 205 x 172	Full span GFRP plate removed
FD	1425 x 205 x 186	Fire damaged between point loads

Note: Beam dimensions are given in a c/c span x width x depth format.

3.2 Experimental Test Setup and Instrumentation

The most damaging bridge fires are commonly caused by tankers spilling flammable liquids near or below a bridge, with hydrocarbon fuels being the most relevant (Garlock et al. 2012; Peris-Sayol et al. 2017). The fire test described herein was intended to be experimental in nature to explore the appropriate GFRP–concrete response resulting from a fire-damaged state. The pool fire used to damage Beam FD had a pan diameter of 300 mm, burned 1.6 L of heptane at 0.11 L=min, and had a continuous flame height of approximately 0.5 m. The beam was supported 500 mm above the base of the fuel pan. See Drysdale (2011) for information on calculating thermal exposures from pool fires. A total burn time of approximately 15 min was used to inflict minor fire damage to the beam and study the underlying mechanics. The authors acknowledge this is a relatively small fire exposure; however, the ultimate goal is to direct future tests where large-scale fires will be considered. A small fire exposure allows the GFRP response to be studied without the introduction of complicating factors, such as concrete degradation. Short-duration hydrocarbon pool fires for structural testing have been used by Byström et al. (2014). Elsewhere in the literature, modeling by Aziz and Kodur (2013) and by Kodur et al. (2017) of composite

concrete-steel bridge decks and unprotected steel bridge girders, respectively, suggests failure times for hydrocarbon fires of under 25 min, albeit under more severe fire exposures. For the purpose of invoking a damage state, the small fire exposure described herein is assumed to be suitable.

Moreover, in Canada and many other jurisdictions where the GFRP stay-in-place formwork is marketed, there is no specific fire endurance requirement for bridges. European and American/ Canadian bridge design standards (Eurocode 1 Part 2 and AASHTO/ CSA, respectively) do not discuss bridge fires, and European fire design standards (Eurocode 1 Part 1-2) apply to buildings, not bridges, where typical spans and structural systems vary significantly (CSA 2014; AASHTO 2015; CEN 2002, 2003). This is a well-described issue that has been discussed by many researchers (Garlock et al. 2012; Peris-Sayol et al. 2017). As far as the authors are aware, the only national standard that provides information on the fire endurance requirements of bridges is National Fire Protection Association (NFPA) 502: Standard for Road Tunnels, Bridges, and Other Limited Highways, which specifies the general method to select design fires for bridges longer than 300 m (NFPA 2014). This standard recommends that design fires for bridges be chosen based on the potential fire produced by the types of vehicles passing under the bridge in question (NFPA 2014). Local authorities or bridge owners may specify fire resistance on a case-by-case basis, but this is not the international norm based on the information detailed earlier.

Based on NFPA 502's recommendation to consider the design fires of vehicle types that pass under a bridge, the fire scenario in this manuscript (although admittedly small) may be considered realistic depending on the scale of the bridge in question (NFPA 2014). More generally, a fast and hot fire should be in the range of considered design fires when carrying out a full performance-based design of a bridge.

Simulated fire damage to Specimens SD1, SD2, SD3, and SDF was applied in the laboratory over a month after casting by cutting on either side of the web-base joint and prying off the base plate. No concrete was damaged in the removal of the GFRP base plate. All specimens except Specimen FD were tested approximately 50 days after casting. Due to laboratory restrictions, the burning and testing of Specimen FD occurred approximately 3 months after the testing of all other specimens.

After the simulated and fire damage was applied to each beam, they were tested in simply supported, four-point monotonic bending. Fig. 5 gives the typical load configuration for each test and the setup for the pool fire. This loading configuration was used to quantify the flexural performance of the GFRP stay-in-place formwork. The beams spanned 1,425 mm from support centers with 125 mm overhangs at either side. Point loads were spaced evenly along the span at 475 mm.

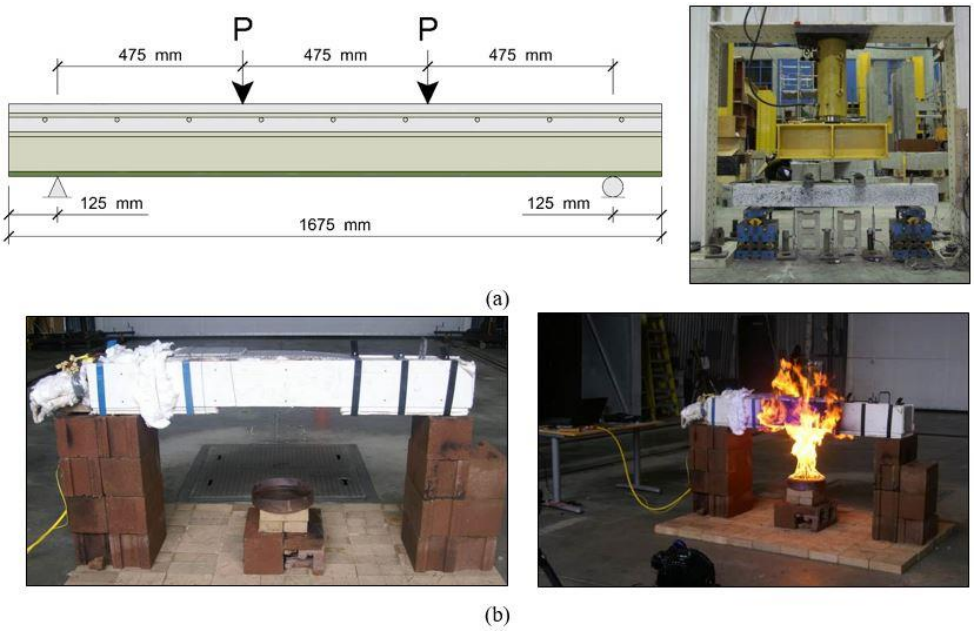

Fig. 5. (a) Typical experimental test setup and loading configuration; (b) pool fire burn setup.

Specimen FD was tested at ambient temperature after the fire was exhausted to assess the residual capacity of the beam postfire. Heating while loading was beyond the scope of this paper; however, the authors acknowledge its relevance, especially in the context of GFRP materials, where the effect of the glass transition temperature is critical (Gales and Green 2015; Del Prete et al. 2015). In-fire tests do fall within the scope of the authors' and others' future work.

A variety of instrumentation techniques were used in this study to monitor the responses of the test specimens. Three linear voltage displacement transducers (LVDTs) were used to measure the deflections along the length of each beam. GFRP-rated strain gauges were installed at the quarter spans and midspan of the T-Up rib flanges to monitor changes in rib strain relative to damage extents. In general, FRPs can be very susceptible to high temperatures, especially in the case of externally bonded FRP reinforcements where adhesion can be compromised by heating as described in Del Prete et al. (2015). Specimen FD was instrumented with two thermocouples placed on the interior side of the GFRP base plate at the midspan to record the GFRP–concrete bond temperature. Two additional thermocouples were used to monitor the ambient air temperature in the laboratory and the temperature of the GFRP soffit. All thermocouples were simple k-type gauges and only measured point temperatures and are illustrated in Fig. 6 showing temperature versus time.

Both thermocouples on the interior side of the GFRP base plate measured peak temperatures of less than 100°C, while the gas temperature at the exposed surface measured a peak of approximately 900°C. A numerical study would be useful to investigate the heat transfer across the GFRP–concrete interface and assess the degree of heating the concrete can sustain beyond this layer. Because the concrete temperature adjacent to the GFRP soffit was below 100°C, there exists negligible degradation of concrete strength due to heating at any point in the concrete and spalling could not have occurred. This result is significant because it validates the authors'

assumption that only the GFRP formwork would be damaged in a fire of this severity. This assumption was the basis for only removing sections of the GFRP forms and not damaging the adjacent concrete or the embedded GFRP rib. It should be noted that this method of simulated damage is only valid for pool fires of the extent and severity described. More severe fires will transfer additional heat to the concrete and cause severe material degradation, expansion, or spalling due to temperatures well beyond 100°C. Tests that investigate heat transfer to the concrete are within the scope of the authors' future experimental and numerical research plans.

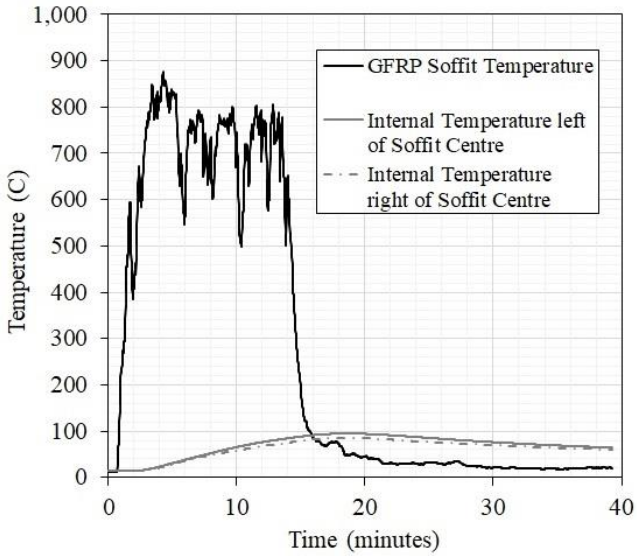

Fig. 6. Time temperature history for beam FD.

3.3 Direct Bond Shear Tests

The adhesive bond between the GFRP formwork and concrete is the main component of shear transfer between materials, with friction representing a secondary component. This shear transfer is vital to developing composite action between the concrete and the GFRP reinforcement. An experimental program was developed to test the GFRP–concrete bond shear strength after exposure to increasing bond temperatures, as observed in the previously described beam tests. This experimental program is intended to provide insight on potential GFRP resin post-curing or other localized bond-altering effects as a result of heating.

The direct shear test program consisted of 16 small-scale specimens of GFRP formwork samples cast between two concrete blocks to recreate the bond between the GFRP formwork and a concrete bridge deck. The concrete also provides a loading surface for the apparatus. The concrete mix design, strength, and moisture were consistent and verified with the ambient concrete properties of the beam tests. The samples were heated to a range of internal bond temperatures near those experienced by Beam FD tested herein, as recorded by thermocouples at the GFRP–concrete interface. The GFRP–concrete bond in Beam FD was measured to have a peak temperature of just under 100°C. Sample temperatures varied between 100°C and 200°C in increments of 25°C. This temperature range encompasses the bond temperatures recorded in Beam FD and beyond. Ambient tests were conducted to provide a baseline. Samples were heated

at a rate of 5°C=min to the desired temperature in a laboratory oven and held for 2 h to ensure uniform temperature. Heated samples were allowed to cool to ambient temperature and tested in a direct shear apparatus using an Instron 5882 loading actuator at a loading rate of 0.25 mm=min. Fig. 7 shows a typical GFRP–concrete sample in a direct shear apparatus. The authors believe this loading configuration is more representative of the interaction between GFRP formwork and concrete in large-scale than a pullout test. In this study, the orientation of the GFRP fibers and their influence on the bond shear strength were studied by testing half the samples parallel to the GFRP fiber direction and the other half perpendicular to the GFRP fiber direction. The orientation seemed to show little difference in the results. Table 3 outlines the test variables considered.

3.4 Digital Image Correlation

Digital image correlation (DIC) was used to measure displacements and estimate slip at the concrete–GFRP interface. Fig. 8 shows a typical DIC setup in this study. A series of photos are taken during each test at regular intervals with a high-resolution camera. By introducing a speckled paint pattern on the side of the specimen, the movement of points on the surface can be tracked between photos using computer software and deformation values can be obtained. In past studies, DIC proved to be a useful tool for determining displacements, relative movements of concrete and external reinforcements, and other surface deformations (Verbruggen et al. 2016; Destrebecq et al. 2011).

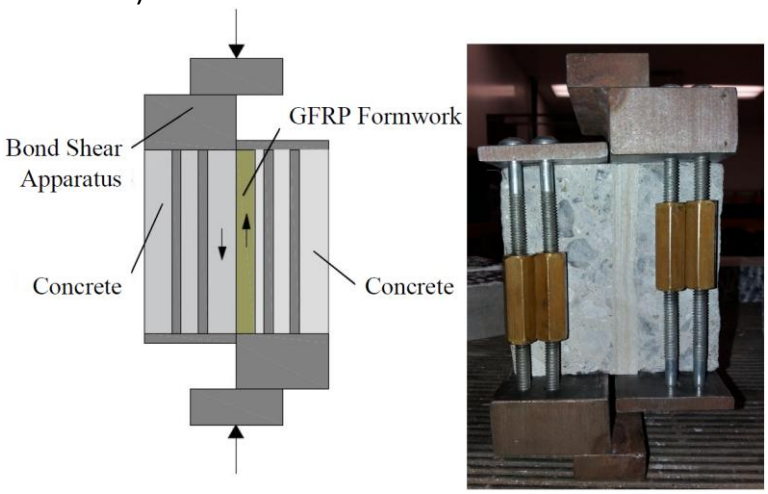

Fig. 7. Direct bond shear test apparatus.

The camera used in this study was a 50-megapixel Canon 5Ds Mark III. The software used in analysis was GeoPIV-RG and MATLAB, which applies interpolation functions to track movement between points of interest in subsequent images. Gales and Green (2015) outline some qualitative errors associated with optical measuring and potential solutions to these issues. The measurement error associated with DIC is on the order of 0.0001 mm, arising from GeoPIV-RG's standard and rotational errors of 0.001 pixels (px) and 0.0001 px, respectively (Blaber et al. 2016). To validate the reliability of the DIC analysis, the calculated results of the vertical deflection at midspan for Beams C1 and FD were compared to the measured values from the LVDTs. Fig. 9 shows a comparison between LVDT and DIC vertical displacement results. These results show the very good agreement between the DIC and LVDT deflections. The slight discrepancies at higher

loads are likely due to out-of-plane beam rotation. Digital image correlation was also applied to measure deformations of the concrete– GFRP direct bond shear tests. Fig. 10 shows the typical test setup for the test series.

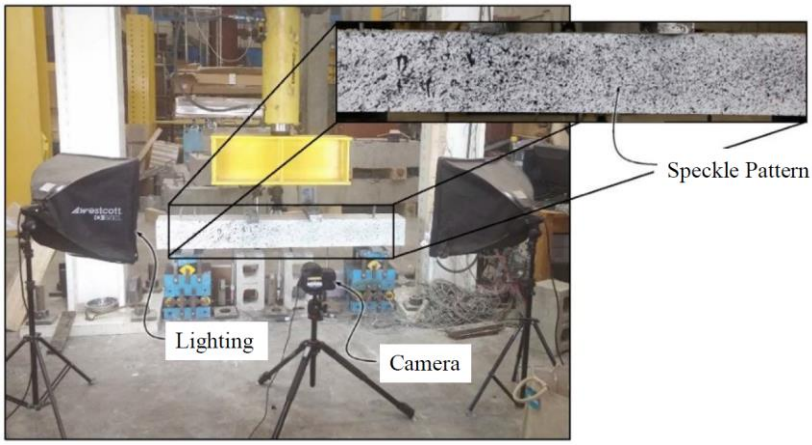

Fig. 8. Digital image correlation test setup and beam speckle pattern.

Table 3. Bond shear test specimens

Shear Direction	Sample	Oven Temp. (°C)	Bond Width (mm)	Bond Height (mm)	Bond Area (mm^2)
Parallel to fibers	A1	20	42	98	4085
	A2	20	53	101	5292
	A3	100	51	102	5184
	A4	100	53	105	5618
	A5	125	52	102	5268
	A6	150	52	101	5321
	A7	175	50	101	5060
	A8	200	49	101	4999
Perpendicular to fibers	B1	20	51	92	4720
	B2	20	55	99	5477
	B3	100	52	104	5366
	B4	100	52	105	5476
	B5	125	53	99	5231
	B6	150	46	98	4473
	B7	175	46	100	4576
	B8	200	48	100	4765

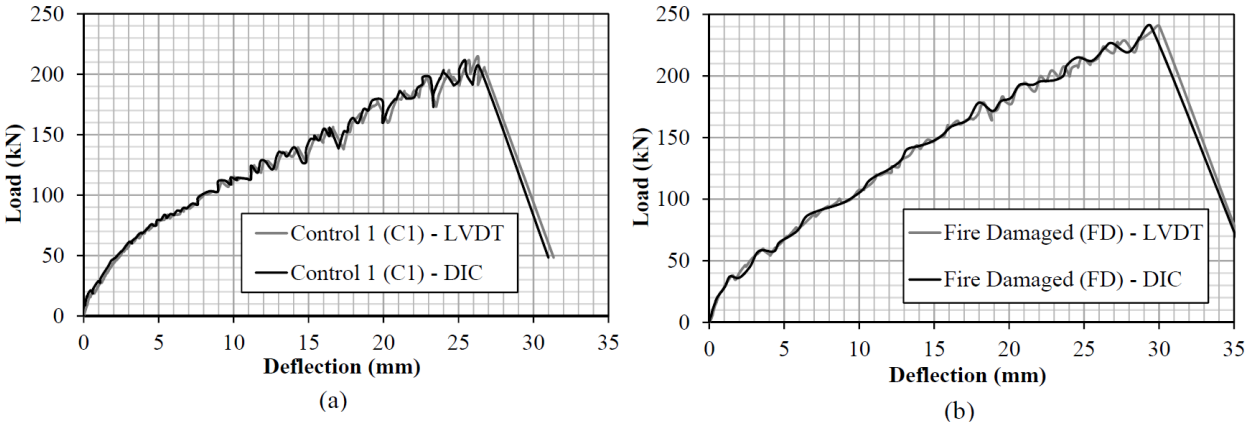

Fig. 9. Comparison of LVDT and DIC midspan deflection response: (a) beam C1 and (b) beam FD.

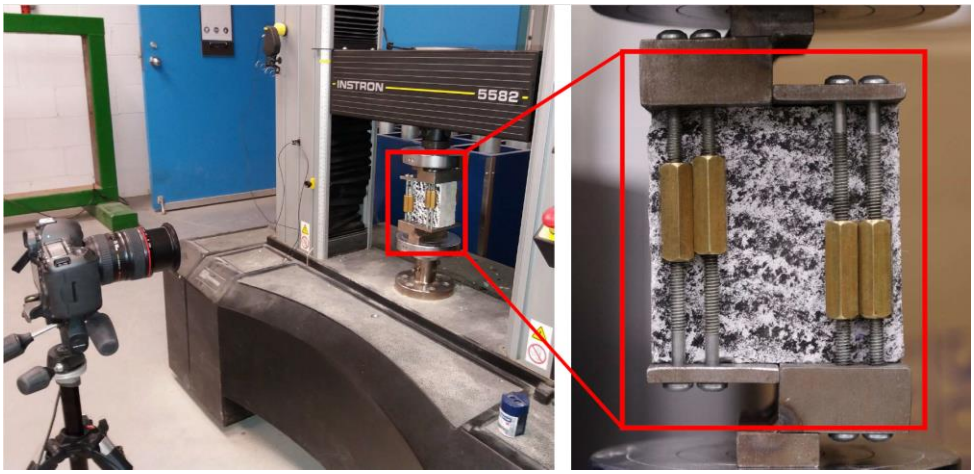

Fig. 10. Digital image correlation test setup for bond shear tests.

A MATLAB script is used to initiate the GeoPIV-RG software. Parameters for photo analysis are input, including an approximate point radius of 50 pixels, an analysis point radius of 25 pixels, a computational limit of 50 iterations, a correlation seed of 0.9, and a correlation limit of 0.9. These parameters influence the picture-to- picture point tracking accuracy. The first photo in the series is used as a baseline for future photos and the points of interest where relative displacements are measured are selected by the user. The GeoPIV-RG software creates acceptable centroids to track based on the selected points. The software runs through all pictures in the test series and tracks the chosen centroids. Relative centroid displacements are output in a MATLAB variable in units of pixels. Results are provided in both the vertical and horizontal directions. A reference image containing a known distance is used to convert pixels to displacements. In this case, the relative vertical displacement between the points selected represents the vertical displacement of the bond.

Fig. 11 shows a typical point selection screen in GeoPIV-RG. This is the same screen used in the beam analysis to determine gap values. The points to be tracked are selected on this screen. In the gap analysis, one point is selected on the GFRP base plate at midspan and one point is selected on the concrete above the GFRP base plate to measure the differential displacement.

For the bond shear tests, two points on opposite sides of the GFRP–concrete shear plane are selected.

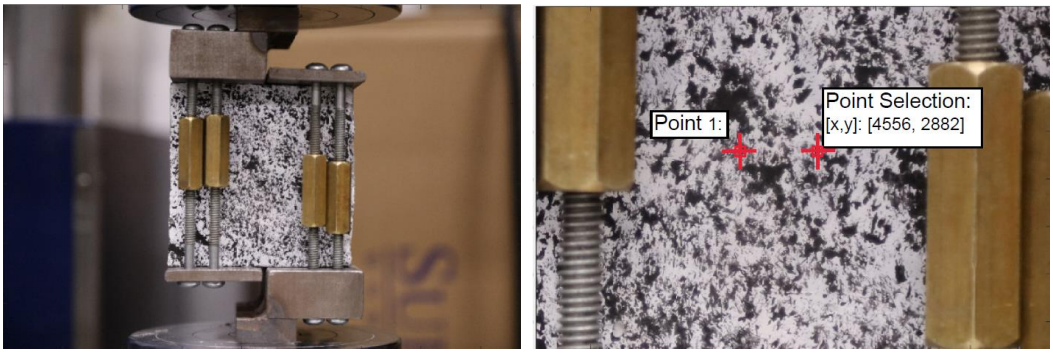

Fig. 11. Point selection screen in GeoPIV-RG for a typical bond shear test.

4. Experimental Results

4.1 Load-Deflection Response

Beams C1 and C2 established a baseline for comparison and verified the effect of downscaling the width of GFRP stay-in-place reinforcement. Specimen C2 was twice the width and had twice the GFRP reinforcement area as C1 but about 10% more than double the ultimate capacity, verifying an approximately linear scaling of capacities with member width. The slight increase in C2 is attributed to concrete confinement by means of the two adjacent ribs. This could also be attributed to tension stiffening of concrete adjacent to the GFRP stay-in-place formwork, which has been observed by Honickman et al. (2009) and Nelson and Fam (2014b). Fig. 12 and Table 4 show the load-deflection responses and key results for all test specimens. The most notable result is that the fire-damaged Beam FD had an approximately 13% higher ultimate capacity than the undamaged control C1. The increase in load carrying capacity is attributed to a concrete prestressing effect due to thermal expansion of the GFRP formwork. This hypothesis is discussed in more detail subsequently. All simulated damage tests had similar load-deflection behaviors except for Beam SD2, which failed at a much lower deflection. Despite having the smallest area of tensile reinforcement remaining, Beam SDF achieved the highest ultimate load and deflection. The damage inflicted on Beam SDF prevented the concentration of stresses at damage boundaries present in all other SD tests and likely delayed the onset of similar failure mechanisms.

Table 4. Summary of experimental beam results.

Beam	Maximum Load (kN)	Maximum Deflection (mm)
C2	475	29.7
FD	240	30.0
C1	212	25.7
SDF	75	27.9
SD1	68	19.9
SD3	62	24.2
SD2	56	15.2

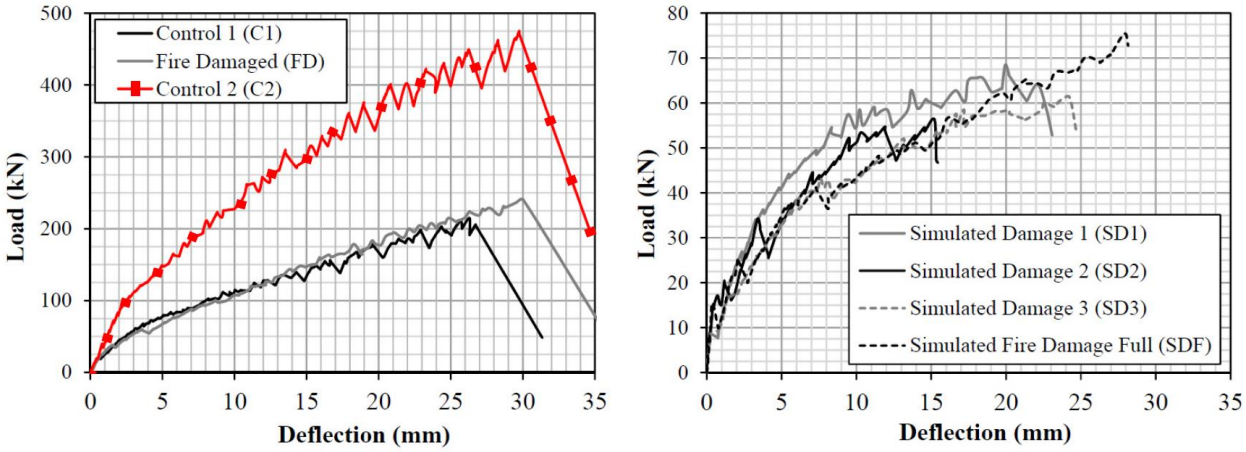

Fig. 12. Beam midspan load-deflection responses: (a) control and fire damaged beams and (b) simulated damage beams.

4.2 Load-Slip Response

An important factor influencing the performance of GFRP stay-in- place formwork bridge decks is composite action between the formwork and the concrete. In practice, bond enhancement can be achieved through a variety of methods to help maintain composite action at higher loads. Some of the common methods include roughening the surface of the GFRP formwork, adhering silica crystals or coarse aggregates to the formwork surface, or applying chemical adhesives prior to casting. In this study, no bond enhancement techniques were used such that the effect of fire on the GFRP could first be understood, avoiding introducing other complicating factors into the study. This was also relevant since one study showed adequate fatigue performance of this system without surface treatment up to five million loading cycles (Richardson et al. 2014).

A loss of composite action is characterized by slipping of the GFRP formwork relative to the concrete and, in more extreme cases, the formation of a vertical gap between the GFRP and concrete. Fig. 13 illustrates the GFRP–concrete slip and gap phenomenon caused by loss of composite action and shows some of the GFRP–concrete slip observed in this study.

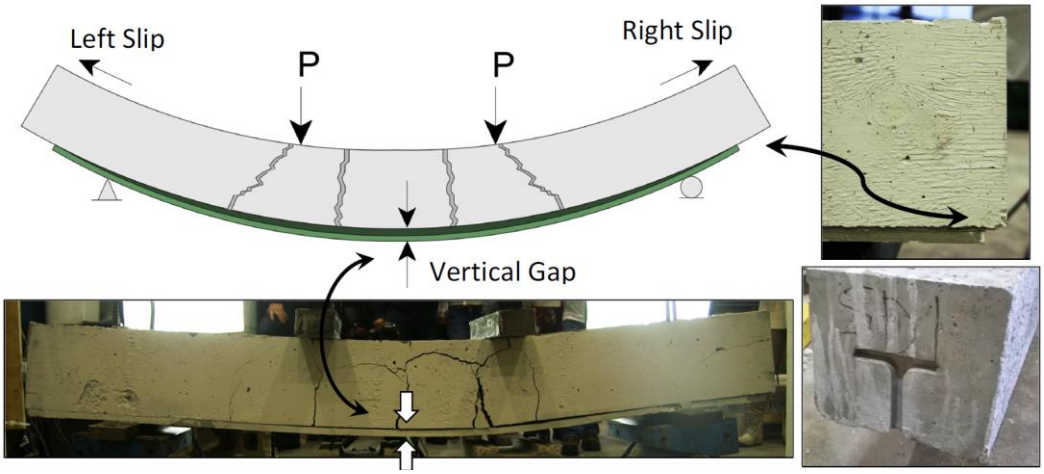

Fig. 13. GFRP-concrete slip and gap behaviours. Specimen C1 is shown.

The relative GFRP–concrete slip for C1, C2, and FD was measured using DIC analysis to understand the GFRP–concrete bond relationship with load carrying capacity. Table 5 shows the results of the slip analysis. The slip phenomenon is quantified in terms of total GFRP–concrete slip (the sum of left and right slips). These values show that the total GFRP end slips at maximum load are similar between Beams C1, C2, and FD despite the damaged state of FD and the greater available bond area in C2. A larger ultimate midspan deflection would result in more relative GFRP–concrete slip due to a larger difference in curvature radii between the concrete and GFRP. Noting this, both Beams FD and C2 had larger ultimate deflections than C1 (approximately 30 mm, 30 mm, and 26 mm, respectively), meaning larger total slips should be observed in these specimens, which is not the case. The additional available bond area in C2 may have resulted in better composite action than in C1. For a more relevant comparison of C1 and FD, the loads and deflections at which the slips are measured can be normalized, as shown in Table 6. The normalized values of 25 mm for deflection and 200 kN for load are arbitrary but were chosen at points closer to the ultimate load. When normalized, there is less total slipping in Beam FD than in C1 when compared at the same load or the same deflection, indicating better composite action in FD. A hypothesized concrete precompression effect due to GFRP heating in FD may have limited the ultimate total end slip. Alternatively, experimental variation between C1 and FD may have resulted in the discrepancies. Fig. 14 shows the time-slip response for Beams C1 and FD.

Table 5. Summary of max relative GFRP-concrete slips for key specimens.

Beam	Maximum Load (kN)	Maximum Slip Left (mm)	Maximum Slip Mid span (mm)	Maximum Slip Right (mm)	Total end slip (mm)
C1	212	4.6	1.8	11.0	15.6
C2	475	7.9	0.2	7.6	15.6
FD	240	7.5	0.3	7.5	15.1

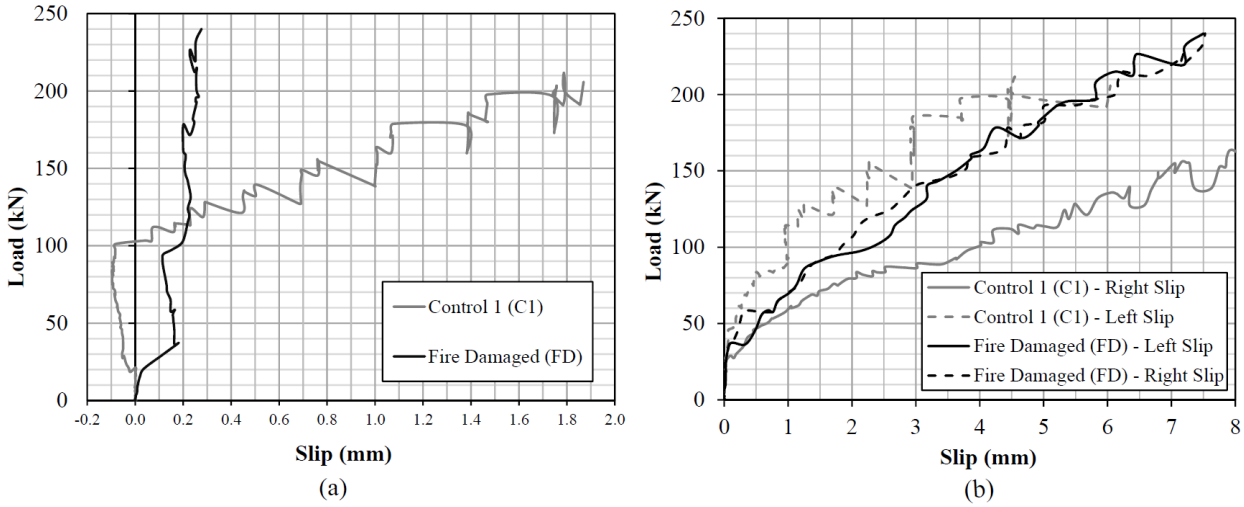

Fig. 14. (a) Midspan horizontal GFRP-concrete slip and (b) left and right horizontal GFRP-concrete slip.

Table 6. Normalized total end slips for FD and C1.

Condition	FD End Slip (mm)	C1 End Slip (mm)
Ultimate Load	15.0	15.6
Normalized for Deflection (25 mm)	12.4	13.6
Normalized for Load (200 kN)	11.9	14.6

The vertical gap between the GFRP and concrete developed at midspan was also measured using DIC analysis to better understand the slip behaviors of Specimens C1 and FD. Specifically, points were selected on either side of the GFRP–concrete interface at midspan and were tracked as the gap formed. The vertical displacements recorded through DIC represent the vertical gap value, while horizontal values represent the slip. Fig. 15 shows the values of the gap that formed between the top of the GFRP base plate and the adjacent concrete at midspan for both beams. These results demonstrate a smaller vertical GFRP separation in Beam FD despite the inflicted fire damage, which implies a stronger GFRP–concrete bond at midspan due to heating and cooling when compared to C1. Although the values in Fig. 15 are within the accuracy of the DIC software, the authors acknowledge that variability between tests could have contributed to the differences discussed at such a small scale.

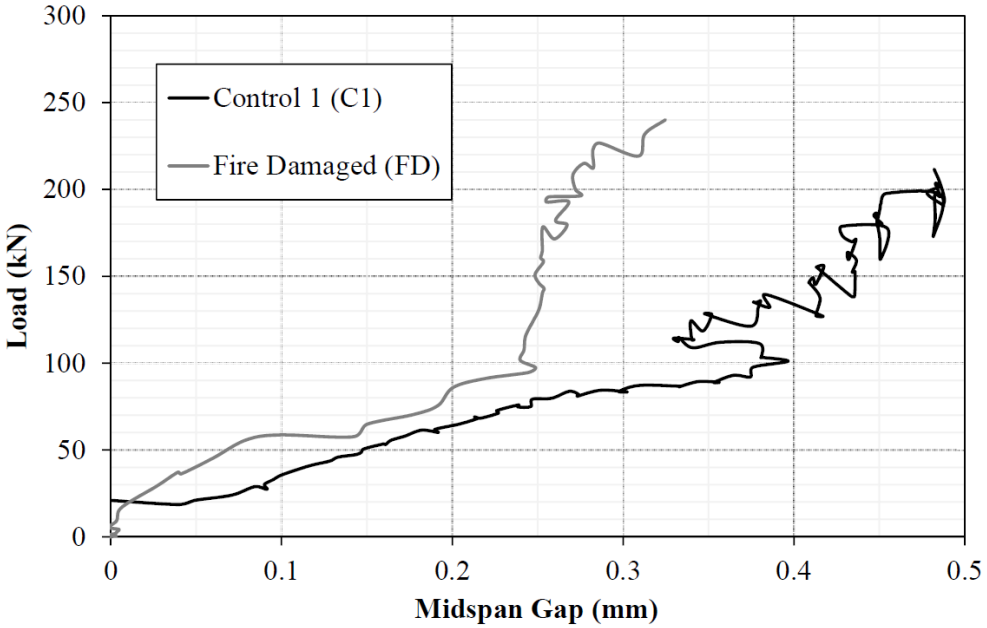

Fig. 15. Vertical GFRP-concrete gap formation at beam midspan.

These data sets further describe better composite action at the midspan of Beam FD than in Beam C1. This indicates that there may be some level of strengthening, possibly due to the heating and cooling of the GFRP formwork, resulting in concrete prestressing. This theory is reinforced by the approximately 13% ultimate load increase in Beam FD compared to C1 and smaller crack widths in Beam FD described subsequently. A similar enhancement was observed by Gooranorimi (2016) in GFRP bars during a study on the performance of RC slabs reinforced with GFRP rebar and exposed to the ASTM E119 standard fire for 120 min. The peak rebar temperature was 115°C, which is similar to the peak interior temperature reached by the GFRP formwork in this study.

The rebar was allowed to cool, removed from the slab, and tested mechanically. Results showed that the horizontal shear strength of the bars increased by roughly 15%, possibly due to resin post-curing (Gooranorimi 2016). Horizontal shear strength (shear in the direction of the fibers) is indicative of resin–fiber interface strength (Gooranorimi 2016). However, the strengthening in this study is not hypothesized to be a result of resin post-curing based on the results of the bond shear tests presented herein.

4.3 Direct Bond Shear Tests

The GFRP–concrete bond shear tests revealed information about the effect of elevated temperatures on the GFRP–concrete interface. In general, there was no evidence of a bond enhancement in direct shear due to resin post-curing or otherwise. There was a clear decrease in failure shear stress as bond temperatures increased. The DIC analysis monitored the bond deformation as shear loading increased. Due to the brittle failure of the test samples, recorded deformations are small but still within the accuracy of the DIC technology, as discussed earlier. Of particular interest was the relative displacement of the GFRP–concrete interface across the bond. Table 7 gives the ultimate loads and stresses for each sample and presents the relative displacements across the GFRP–concrete bond normalized by shear stress at failure. Based on the aforementioned data and physical deformities, Specimen A2 was believed to be defective, likely due to damage or issues encountered during casting, and was omitted from the associated plots. For temperatures at which two samples were tested, the results were averaged in the plots below. Fig. 16 plots the relationship between heated temperature and ultimate shear stress, while Fig. 17 plots the normalized relative GFRP–concrete displacement versus the bond temperature. These plots show that heating the GFRP-concrete interface decreases the ultimate bond shear stress and increases the relative bond deformation when tested in direct shear after the bond temperature has returned to ambient. Although a limited sample size was tested, the relationship between bond deformation and heated temperature appears to be nonlinear; however, additional testing may be required to further study the residual GFRP–concrete bond strength at elevated temperatures.

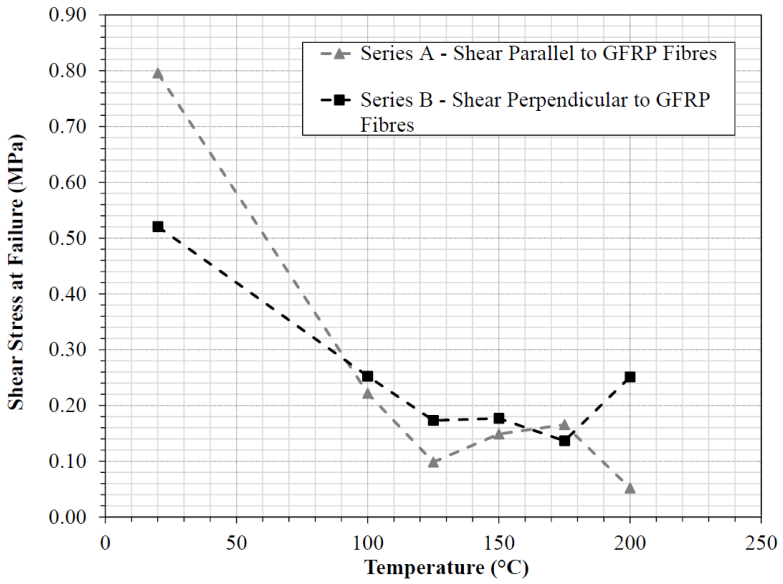

Fig. 16. Ultimate bond shear stress versus heated temperature.

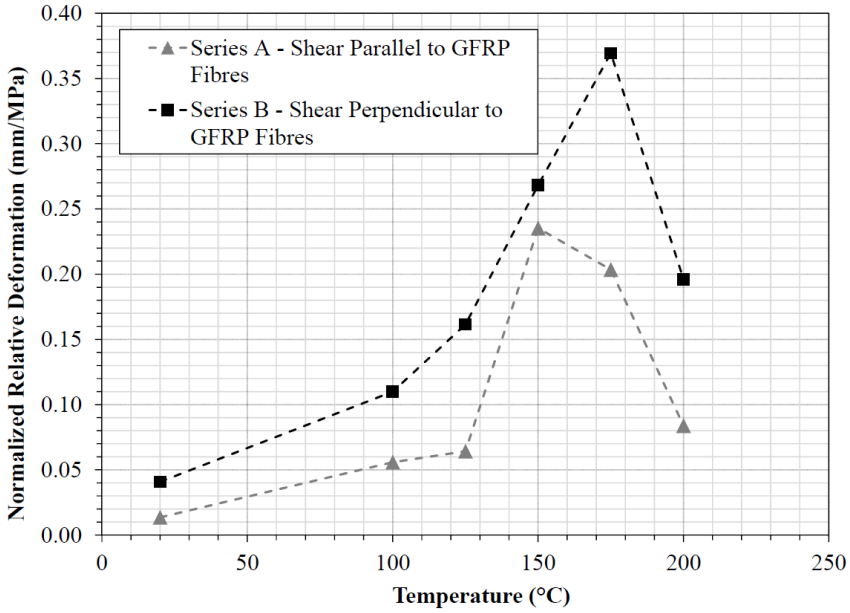

Fig. 17. Normalized GFRP-concrete bond displacement versus heated temperature.

Table 7. Direct bond shear test results

Shear Direction	I.D	Oven Temp. (°C)	Ultimate Load (N)	Ultimate Shear Stress (MPa)	Relative Displacement at Ultimate (mm)	Relative Displacement Normalized by Peak Shear Stress (mm/MPa)
Parallel to GFRP fibers	A1	20	3251	0.796	0.011	0.014
	A2	20	504	0.095	n/a	n/a
	A3	100	1233	0.238	0.018	0.075
	A4	100	1156	0.206	0.008	0.036
	A5	125	519	0.099	0.006	0.064
	A6	150	792	0.149	0.035	0.235
	A7	175	838	0.166	0.034	0.203
	A8	200	260	0.052	0.004	0.084
Perpendicular to GFRP fibers	B1	20	2595	0.550	0.003	0.006
	B2	20	2692	0.491	0.037	0.076
	B3	100	1034	0.193	0.007	0.034
	B4	100	1709	0.312	0.058	0.185
	B5	125	906	0.173	0.028	0.162
	B6	150	791	0.177	0.047	0.268
	B7	175	625	0.137	0.050	0.369
	B8	200	1197	0.251	0.049	0.196

Based on these results, it is concluded that heating the GFRP– concrete interface decreases the bond strength in direct shear and reduces the bond stiffness. This does not exclude the potential for other strengthening effects that could have influenced the largescale beam tests in this study, such as concrete prestressing due to formwork thermal straining, which may still be plausible.

4.4 Crack Behaviour

To better understand the effect of fire damage on load transfer to the GFRP stay-in-place formwork, DIC analysis was applied to measure flexural crack widths in Beams C1, FD, SD3, and SDF. Beams SD1, SD2, and C2 were omitted from the analysis because of their dissimilar damage regions. The widths of the most prominent flexural cracks were measured at the extreme concrete fiber in tension. Fig. 18 shows the relationship between crack widths and applied load. This plot shows that, for the same applied load, Beam FD had smaller crack widths than Beam C1. Additionally, cracking initiated in Beam C1 and FD at approximately 20 and 80 kN, respectively. These results indicate better load transfer to the GFRP stay-in-place formwork in Beam FD than in Beam C1, despite the fire damage inflicted. Alternatively, smaller crack widths in Beam FD could indicate concrete precompression as a result of thermal straining. Despite having a damaged region similar to that of Beam FD, Beam SD3 experienced significantly wider cracks much earlier than other specimens. This is attributed to the hinge formation at the simulated damage boundary, where stress concentrations resulted in a premature GFRP web fracture and exacerbated concrete cracks. The lack of stress concentrations in the formwork of Beam SDF resulted in smaller crack widths than Beam SD3, despite a smaller area of tensile reinforcement.

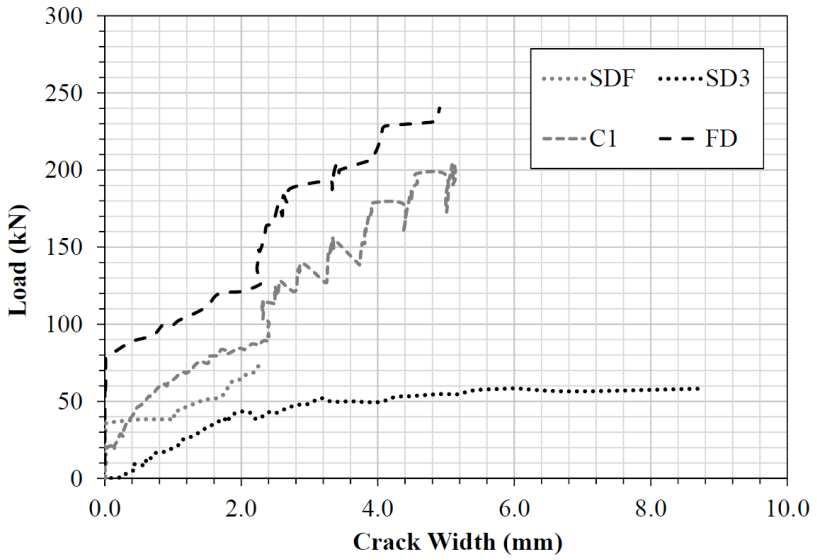

Fig. 18. Flexural crack width at extreme concrete fiber in tension versus load.

4.5 Failure Modes

Two modes of failure were observed between all seven beam tests: (1) separation of the GFRP rib web from the base plate at beam ends in C1, C2, and FD and (2) fracture of the GFRP rib web in SD1, SD2, SD3, and SDF. Loss of composite action between the GFRP formwork and concrete preceded failure in every test. In Beams C1, C2, and FD, partial composite action was maintained during loading, with occasional and large GFRP–concrete slips accompanied by a reduction in load. Even after large slips between the concrete and GFRP, the sustained load was able to re-establish and increase up until failure. Shear failure at the joint of the GFRP web and base plate initiated the separation of the GFRP base plate from the rib web at failure. The fracture length extended approximately from the support to the closest point load. This is shown in Fig. 19.

(a)

(b)

Fig. 19. (a) Beam C2 crack distribution and (b) separation of GFRP base plate from rib web.

Significant flexural cracking was observed in all SD specimens in regions where the GFRP base plate had been removed. Beyond the ultimate load, large portions of cracked concrete fell away from the SD beams and exposed the GFRP T-Up rib. Composite action was not maintained to the same degree as the control and fire-damaged specimens because of the reduced bond surface area. This yielded small and frequent GFRP slips and drops in load. Fracture of the GFRP T-Up rib web occurred at failure. The location of GFRP fracture was dependent on the location of GFRP base plate removal. Where a damage boundary was present, GFRP web fracture occurred at the boundary on the damaged side due to stress concentrations in the GFRP web. With no damage boundaries available in beam SDF, GFRP fracture occurred at approximately midspan. In Beam SD2, a GFRP fracture occurred just outside of the moment span at the damaged boundary. It is hypothesized that stress concentrations at the abrupt damage boundaries in Beam SD2 initiated failure earlier than SDF, which has no abrupt damage boundaries. This is reinforced by the flexural failure of the GFRP web at the damage boundary seen in Fig. 20. Fire scenarios resulting in significant char depths may cause similar stress concentrations if abrupt damage boundaries are present (such as where a GFRP stay-in-place formwork deck meets a bridge girder).

Although the shear resistance provided by the GFRP stay-in-place forms was not a focus of this study, some comparisons can be made with previous ambient temperature tests. One-way bending tests of a 1,220 × 400 × 150 mm concrete slab reinforced with an adhesively bonded, 9.5 mm thick GFRP plate (with no ribs) conducted by Honickman et al. (2009) yielded concrete shear failure and GFRP debonding at the midspan. By comparing these failure modes with those of Beams C1 and C2 in this study, it can be concluded that the GFRP T-Up ribs provide the concrete with significant shear resistance and help mitigate GFRP debonding at midspan.

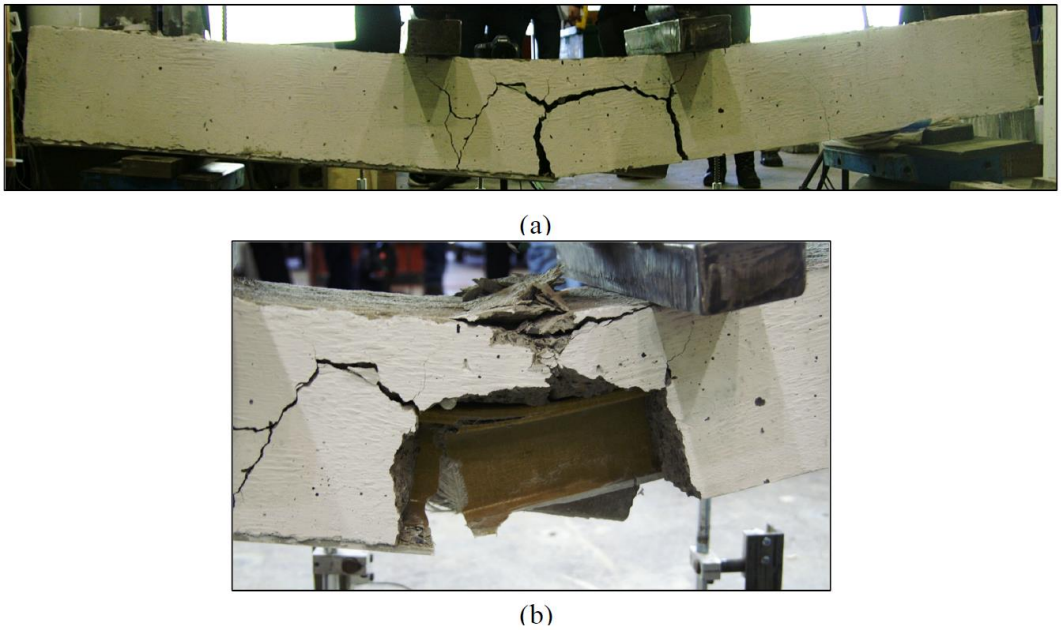

Fig. 20. (a) Beam SD1 crack distribution (post-failure) and (b) GFRP web fracture at a damage boundary.

4.6 Assessment of Simulated Damage

In general, the level of applied simulated fire damage was very conservative for the extent of damage experienced by Beam FD. However, removal of the entire thickness of GFRP plate may still be representative of a specimen inflicted with more severe fire damage depending on the level of concrete heating beyond the GFRP. Regardless of the accuracy of simulated damage in this study, the SD tests still give important information about the behavior of damaged GFRP stay-in-place formwork. The control and simulated damage beams represent boundary conditions in terms of damage depth to the GFRP base plate. For a specific level of damage in the moment span, the corresponding failure mode changes from that of C1 to that of SD3. Beam FD demonstrated the same failure mode and general behavior as C1 so it can be said that the fire damage sustained was insufficient to cause this change in failure mode, but a deeper char layer may induce the alternate failure mechanism.

One research goal was to determine whether the embedded T-Up ribs would bear additional load in the event of damage to the base GFRP plate. Fig. 21 outlines the GFRP rib flange load-strain responses at midspan for all tests. Beam SD2 had all four strain gauges fail and is not shown on the plot. It is observed that there is a large increase in strain developed in the T-Up ribs in the SD tests when compared to C1 and FD. This is likely due to the larger curvatures developed in the SD GFRP formwork and reduced composite action that eventually led to GFRP fracture. Beam SDF had the highest capacity of all simulated damaged beams, suggesting it may be more beneficial to have a uniform region of damage instead of discrete damage boundaries. The strains in C1 and FD are of the same order of magnitude. The rib flange of Beam FD shows a decrease in a stiffness when compared to C1 due to the reduced area of GFRP reinforcement from fire damage and an extended zone of pyrolysis. The measured rib strains are compressive due to the loss of composite action between the GFRP formwork and the concrete. As demonstrated in Fig. 22, as composite action is lost, a strain discontinuity is created between the strain distributions

of the concrete and GFRP, denoted by ε_{slip}. For a full loss of composite action, the neutral axis of the GFRP is given by the centroid of the GFRP cross section and the reinforcement bends independently of the concrete. The strains developed in the T-Up ribs provide an important conclusion about the performance of GFRP stay-in-place formwork in fire conditions in that, for fire scenarios where the embedded ribs are undamaged (which is the vast majority of cases), the ribs provide a redundancy to the system.

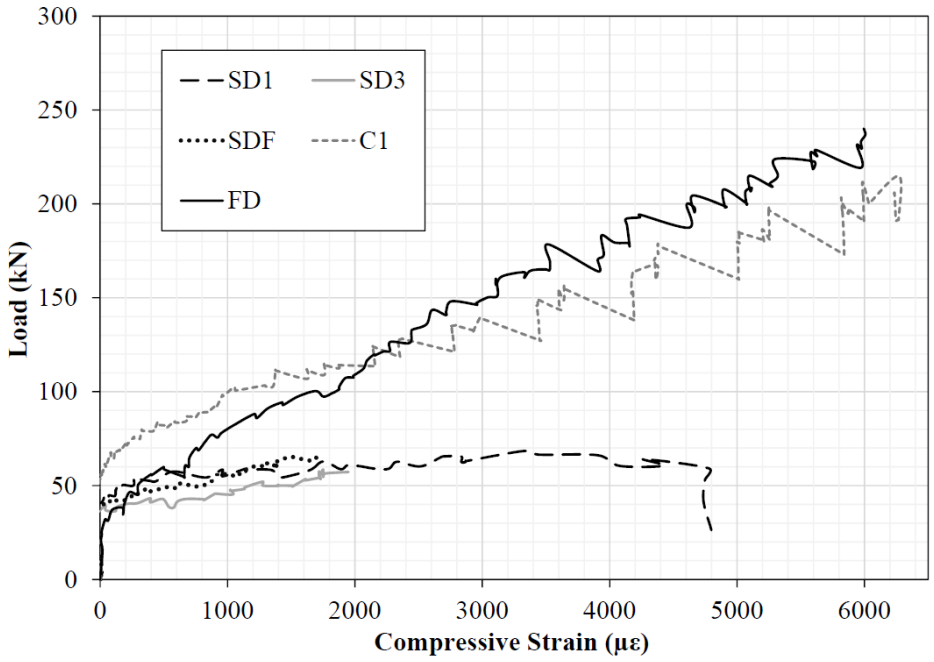

Fig. 21. T-Up rib flange compressive strain response at midspan.

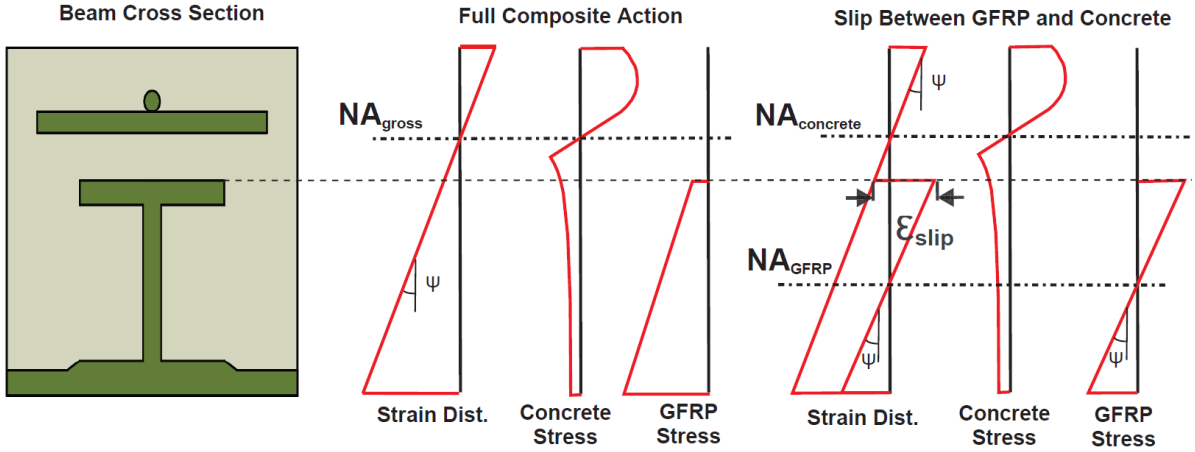

Fig. 22. T-Up rib strain distribution due to GFRP-concrete slip. NA: neutral axis of cross-section. Adapted from Nelson and Fam 2014b.

4.7 Assessment of Fire Damage

Beam FD performed better than suggested by Gales et al. (2016) under exposure to the pool fire. A char layer extended approximately 2 ± 0.5 mm or 15% into the exposed 13.7 mm thick GFRP base plate as measured in six locations across the damaged soffit. The small variation in char

depth (0.5 mm) over the damaged region of Beam FD provides the authors with confidence that heating was moderately uniform along the exposed region. The variations in char depth could be due to flame dispersion effects. It should be noted that the region directly beneath the char layer still contributes structurally to the member but may have undergone some level of chemical change, including pyrolysis during heating. This layer will have altered postfire mechanical properties based on chemical change from partial GFRP decomposition. Delamination of outer laminates occurred on the charred GFRP surface. The GFRP experienced flame-out almost immediately after the pool fire fuel was exhausted. This suggests that a more severe fire may be required to sustain a flame on the GFRP surface after flame-out. Fig. 23 shows the delamination and charring of the base plate observed during the test.

Fig. 23. Delaminated pyrolysis/char layer on GFRP base plate soffit.

5. Conclusions and Future Research

The goal of this project was to gain an understanding of the behavior of GFRP stay-in-place T-Up structural formwork exposed to localized fire damage, within the context of concrete bridge deck applications. Fire damage was simulated in a series of bridge deck sections reinforced with GFRP formwork by physically removing the GFRP base plate. Comparisons were made to undamaged control beams and a beam damaged by a heptane pool fire. The effect of elevated temperatures on the GFRP–concrete bond was also investigated in direct shear.

5.1 Contributions to the State of the Art

This paper has presented first-stage research into the postfire performance of concrete beams reinforced with GFRP stay-in-place formwork intended for bridge deck construction. Despite the limitations outlined throughout this article, the information presented herein offers novel insights into a previously unexplored damage state for this specific structural system. Specifically, this manuscript has:

- conducted the first, to the knowledge of the authors, high-temperature damage test on a GFRP stay-in-place formwork structural system that recorded GFRP surface temperatures exceeding 800°C, reported on the observed material and mechanical behaviors, and

identified areas requiring future research, specifically, the potential for flexural strengthening resulting from low heating;
- examined and drawn conclusions about the influence of both minor-fire and severe physical damage on the mechanical behavior of the GFRP system using four-point bending tests not considered in past mechanical research involving this structural configuration; and
- performed the initial study with a novel series of direct bond shear tests to further examine the effect of high temperatures on the concrete-GFRP interface which ruled out a bond strengthening phenomenon and gave badly needed information on the bond stiffness deterioration.

5.2 Limitations of the Heating Exposure Used in this Study

This study focused on the mechanical behavior of GFRP stay-in-place formwork beams under a variety of damage states, including an arbitrary fire-damaged condition. The fire scenario presented in this paper represented the extent of the authors' available resources and was used solely for the purpose of invoking a measurable postfire damaged state on the GFRP stay-in-place formwork system in order to study the mechanical response. The authors by no means advocate such small-fire exposure in the context of bridge fire safety studies where realistic fires are orders of magnitude more severe than that presented herein, specifically with regard to the heat release rate and duration. It is also not the authors' intention that the time–temperature data presented for the surface of the GFRP be interpreted as a realistic bridge fire scenario; its inclusion is simply to provide context to the fire-damaged state of a specimen, not set a precedent for future tests. However, it is the authors' opinion that the use of open-flame pool fires in structural fire testing, especially in connection with bridge fires where hydrocarbon pool fires are common, is an approach with merit when applied properly in scale and can yield behaviors not necessarily realized in other test methods. This paper is intended to act as a precursor to future studies where densely instrumented tests on appropriately scaled specimens with realistic hydrocarbon fires will be considered, coupled with well-controlled furnace tests that will both enable accurate modeling endeavors.

5.3 Future Work and Recommendations

The following topics were identified by the authors as potential areas for future work:

- investigation of the bond behavior of concrete and GFRP formwork in elevated temperatures at larger scales;
- investigation of concrete pre-compressive action as a result of GFRP formwork heating and cooling;
- simultaneous heating and loading of concrete–GFRP formwork systems to identify load-induced thermal straining effects (LITS) and creep effects;
- exposure of large-scale concrete–GFRP formwork systems to a variety of design fires including standard fires; and
- development of numerical models to account for secondary heating effects on concrete–GFRP formwork systems as well as full material characterization.

5.4 Conclusions

Conclusions from this test program are as follows:

1. The capacity increase present in fire-damaged beams when compared to the undamaged control is hypothesized to be a result of concrete precompression developed from the heating and cooling of the GFRP base plate.

2. There is no apparent strengthening effect from heating the GFRP–concrete bond and loading in direct shear. There is an evident and nonlinear decrease in bond shear stiffness as the heated bond temperature increased.

3. Removal of the full thickness of the GFRP base plate was an overly conservative approximation of the fire damage sustained by the specimen but may be accurate for more severe fires depending on the level of concrete heating.

4. The fire damage sustained was insufficient to reduce the ultimate load or change the failure mode of the specimen when compared to the undamaged control. The embedded T-rib is also protected from fire damage and provides redundancy to the system.

5. Despite a char thickness of about 15% of the base thickness, the GFRP base plate was able to protect the adjacent concrete from temperatures of over 100°C.

6. There is an approximately linear relationship between beam width and the ultimate load/strains developed in GFRP T-Up rib flanges at the scales studied, but confinement and tension stiffening may affect wider members with multiple ribs, causing about 10% increased strength per unit width.

7. It may be less detrimental to have symmetric and uniform areas of damage on the GFRP base plate when compared to abrupt or asymmetric damage boundaries due to the introduction of stress concentrations in the GFRP web.

8. The thermal thickness of GFRP base plates is a critical factor in fire resistance and prevents upscaling of small-scale GFRP stay-in-place formwork fire tests.

9. No sustained flaming was observed on the GFRP soffit after the pool fire was exhausted.

10. For the fire conditions studied, a stay-in-place formwork reinforced bridge deck would likely be repairable with minimal closure time due to the same level of flexural capacity.

This study was intended to direct the focus of future studies and provide an understanding of the effect of fire on GFRP stay-in-place formwork–concrete systems. More experiments of this nature should be conducted to confirm the conclusions drawn herein. These conclusions suggest that GFRP stay-in-place formwork hold great potential for civil engineering applications, but the

performance and behavior of GFRP materials at elevated temperatures must be better understood.

6. Acknowledgements

The authors would like to acknowledge the technical staff at Carleton University. Beth Weckman and Matt DiDomizio from Waterloo's Fire Safety Engineering Laboratory are greatly thanked for their assistance with this study. Material contributions from Queen's University and V-ROD Canada are gratefully acknowledged. Seth Gatien of Carleton University is acknowledged for his work on GeoPIV-RG. Matthew Smith of Entuitive is thanked for his comments on this paper. Funding for the principal author was provided by the Natural Sciences Engineering Research Council's undergraduate research program and Carleton University's I-CUREUS undergraduate program.

7. References

AASHTO. 2015. *LRFD bridge design specifications*. Washington, DC: AASHTO.

Aziz, E., and V. Kodur. 2013. "An approach for evaluating the residual strength of fire exposed bridge girders." *J. Constr. Steel Res.* 88: 34–42. https://doi.org/10.1016/j.jcsr.2013.04.007.

Bai, Y., T. Keller, J. R. Correia, F. A. Branco, and J. G. Ferreira. 2010. "Fire protection systems for building floors made of pultruded GFRP profiles—Part 2: Modeling of thermomechanical responses." *Composites Part B* 41 (8): 630–636. https://doi.org/10.1016/j.compositesb.2010.09.019.

Blaber, J., S. A. Stanier, W. A. Take, and D. J. White. 2016. "Improved image-based deformation measurement for geotechnical applications." *Can. Geotech. J.* 53 (5): 727–739. https://doi.org/10.1139/cgj-2015-0253.

Boles, R., M. Nelson, and A. Fam. 2015. "Durability of bridge deck with FRP stay-in-place structural forms under freeze-thaw cycles." *J. Compos. Constr.* 19 (4): 04014070. https://doi.org/10.1061/(ASCE)CC.1943-5614.0000531.

Byström, A., J. Sjöström, U. Wickström, D. Lange, and M. Veljkovic. 2014. "Large scale test on a steel column exposed to localized fire." *J. Struct. Fire Eng.* 5 (2): 147–160. https://doi.org/10.1260/2040-2317.5.2.147.

CEN (European Committee for Standardization). 2002. Actions on structures—Part 1–2: General actions—Actions on structures exposed to fire. Eurocode 1. Brussels, Belgium: CEN.

CEN (European Committee for Standardization). 2003. Actions on structures—Part 2: Traffic loads on bridges. Eurocode 1. Brussels, Belgium: CEN.

Correia, J. R., Y. Bai, and T. Keller. 2015. "A review of the fire behaviour of pultruded GFRP structural profiles for civil engineering applications." *Compos. Struct.* 127: 267–287. https://doi.org/10.1016/j.compstruct.2015.03.006.

Correia, J. R., F. A. Branco, J. G. Ferreira, Y. Bai, and T. Keller. 2010. "Fire protection systems for building floors made of pultruded GFRP profiles. Part 1: Experimental investigations." *Composites Part B* 41 (8): 617–629. https://doi.org/10.1016/j.compositesb.2010.09.018.

Correia, J. R., M. M. Gomes, J. M. Pires, and F. A. Branco. 2013. "Mechanical behaviour of pultruded glass fiber reinforced polymer composites at elevated temperature: Experiments and model assessment." *Compos. Struct.* 98: 303–313. https://doi.org/10.1016/j.compstruct.2012.10.051.

CSA (Canadian Standards Association). 2014. Canadian highway bridge design code. CAN/CSA-S6. Rexdale, Canada: CSA.

Del Prete, I., A. Bilotta, and E. Nigro. 2015. "Performances at high temperature of RC bridge decks strengthened with EBR-FRP." *Composites Part B* 68: 27–37. https://doi.org/10.1016/j.compositesb.2014.08.011.

Destrebecq, J., E. Toussaint, and E. Ferrier. 2011. "Analysis of cracks and deformations in a full scale reinforced concrete beam using a digital image correlation technique." *Exp. Mech.* 51 (6): 879–890. https://doi.org/10.1007/s11340-010-9384-9.

Drysdale, D. 2011. *An introduction to fire dynamics*. 3rd ed. Chichester, UK: Wiley.

Fam, A., R. Boles, and M. Robert. 2016. "Durability in a salt solution of pultruded composite materials used in structural sections for bridge deck applications." *J. Bridge Eng.* 21 (1): 04015032. https://doi.org/10.1061/(ASCE)BE.1943-5592.0000768.

Gales, J., and M. Green. 2015. "Optical characterization of high temperature deformation in novel structural materials." In Proc., 14th Int. Conf. on Fire and Materials, 626–640. London: Grayson Franks Ltd.

Gales, J., N. Nagy, and B. Weckman. 2016. "Improving fire safety of glass fiber reinforced polymers for bridge infrastructures." In Proc., Interflam 2016: 14th Int. Conf. and Exhibition on Fire Science and Engineering, 747–752. Windsor, UK: Royal Holloway College.

Garlock, M., I. Paya-Zaforteza, V. Kodur, and L. Gu. 2012. "Fire hazard in bridges: Review, assessment and repair strategies." *Eng. Struct.* 35: 89–98. https://doi.org/10.1016/j.engstruct.2011.11.002.

Gibson, A. G., Y. S. Wu, J. T. Evans, and A. P. Mouritz. 2006. "Laminate theory analysis of composites under load in fire." *J. Compos. Mater.* 40 (7): 639–658. https://doi.org/10.1177/0021998305055543.

Gooranorimi, O. 2016. "Investigation of bond, microstructure and post-fire behavior of GFRP reinforcement for concrete." Ph.D. dissertation, Dept. of Civil, Architectural, and Environmental Engineering, Univ. of Miami.

Honickman, H., M. Nelson, and A. Fam. 2009. "Investigation into the bond of glass fiber-reinforced polymer stay-in-place structural forms to concrete for decking applications." *Transp. Res. Rec.* 2131 (1): 134–144. https://doi.org/10.3141/2131-13.

Kodur, V. K., E. M. Aziz, and M. Z. Naser. 2017. "Strategies for enhancing fire performance of steel bridges." *Eng. Struct.* 131: 446–458. https://doi.org/10.1016/j.engstruct.2016.10.040.

Morgado, T., J. R. Correia, A. Moreira, F. A. Branco, and C. Tiago. 2015. "Experimental study on the fire resistance of GFRP pultruded tubular columns." *Composites Part B* 69: 201–211. https://doi.org/10.1016/j.compositesb.2014.10.005.

Morgado, T., N. Silvestre, and J. R. Correia. 2018a. "Simulation of fire resistance behaviour of pultruded GFRP beams—Part I: Models description and kinematic issues." *Compos. Struct.* 187: 269–280. https://doi.org/10.1016/j.compstruct.2017.12.063.

Morgado, T., N. Silvestre, and J. R. Correia. 2018b. "Simulation of fire resistance behaviour of pultruded GFRP beams—Part II: Stress analysis and failure criteria." *Compos. Struct.* 188: 519–530. https://doi.org/10.1016/j.compstruct.2017.12.064.

Nelson, M., and A. Fam. 2013. "Structural GFRP permanent forms with T-shape ribs for bridge decks supported by precast concrete girders." *J. Bridge Eng.* 18 (9): 813–826. https://doi.org/10.1061/(ASCE)BE.1943-5592.0000418.

Nelson, M., and A. Fam. 2014a. "Full bridge testing at scale constructed with a novel FRP stay-in-place structural forms for concrete deck." *Constr. Build. Mater.* 50: 368–376. https://doi.org/10.1016/j.conbuildmat.2013.09.056.

Nelson, M., and A. Fam. 2014b. "Modeling of flexural behavior and punching shear of concrete bridge decks with FRP stay-in-place forms using the theory of plates." *J. Eng. Mech.* 140 (12): 04014095. https://doi.org/10.1061/(ASCE)EM.1943-7889.0000813.

NFPA (National Fire Protection Association). 2014. Standard for road tunnels, bridges, and other limited highways. NFPA 502. Quincy, MA: NEPA.

Peris-Sayol, G., I. Paya-Zaforteza, S. Balasch-Parisi, and J. Alós-Moya. 2017. "Detailed analysis of the causes of bridge fires and their associated damage levels." *J. Perform. Constr. Facil.* 31 (3): 04016108. https://doi.org/10.1061/(ASCE)CF.1943-5509.0000977.

Richardson, P., M. Nelson, and A. Fam. 2014. "Fatigue behavior of concrete bridge decks cast on GFRP stay-in-place structural forms." *J. Compos. Constr.* 18 (3): A4013010. https://doi.org/10.1061/(ASCE)CC.1943-5614.0000432.

Verbruggen, S., S. De Sutter, S. Iliopoulos, D. G. Aggelis, and T. Tysmans. 2016. "Experimental structural analysis of hybrid composite-concrete beams by digital image correlation (DIC) and acoustic emission (AE)." *J. Nondestr. Eval.* 35 (1): 1–10. https://doi.org/10.1007/s10921-015-0321-9.

Yanes-Armas, S., J. de Castro, and T. Keller. 2016. "System transverse in-plane shear stiffness of sultruded GFRP bridge decks." *Eng. Struct.* 107: 34–46. https://doi.org/10.1016/j.engstruct.2015.11.003.

Yanes-Armas, S., J. de Castro, and T. Keller. 2017. "Rotational stiffness of web-flange junctions of pultruded GFRP decks." *Eng. Struct.* 140: 373–389. https://doi.org/10.1016/j.engstruct.2017.03.003.